

AUTOMATIC OPTIC DISK DETECTION FROM LOW CONTRAST RETINAL IMAGES OF ROP INFANT USING GVF SNAKE

Viranee Thongnuch* and Bunyarit Uyyanonvara*

Received: Jan 22, 2007; Revised: Jun 19, 2007; Accepted: Jun 25, 2007

Abstract

Reliable and efficient optic disk localization and segmentation are important tasks in automated retinal screening. General-purpose edge detection algorithms often fail to segment the optic disk (OD) due to fuzzy boundaries, inconsistent image contrast or missing edge features, especially in infants' retinal images where the image acquisition process has to be very quick and in low light conditions. This paper presents an algorithm for segmentation of optic disk boundary in low-contrast images. The optic disk localization is achieved using segmentation by a deformable contour model (or Snake) with gradient vector flow (GVF) as an external force. The first Snake is placed at a location very close to the center of the optic disk approximated by a PCA-based model. The algorithm is evaluated using 50 retinal images from infants with retinopathy of prematurity (ROP) condition. The results from the GVF method were compared with conventional optic disk detection using a 2D Circular Hough Transform and later verified with hand-drawn ground truth. The result is quite successful with the accuracy of 85.34%.

Keywords: Optic disk, retinopathy of prematurity, segmentation, PCA, Snake, gradient vector flow

Introduction

Retinopathy of Prematurity (ROP) is a developmental disease of the eye that affects premature infants. When a premature baby is born, the retinal blood vessels have not completed their development. In cases of patients with ROP, the blood vessels stop growing and new, abnormal blood vessels grow instead of the normal ones. The most severe complication of this disease is bilateral blindness in early childhood.

Precise localization of the optic disk boundary is an important sub-problem of higher

level problems in ophthalmic image processing. Specifically, in proliferative diabetic retinopathy, fragile vessels develop in the retina, largely in the OD region, in response to circulation problems created during earlier stages of the disease. If the optic disk has been identified, the position of areas of clinical importance such as the fovea may be determined. Moreover, OD detection is fundamental for establishing a frame of reference within the retinal image and is, thus, important for any image analysis application.

*School of Information and Computer Technology Sirindhorn International Institute of Technology, Thammasat University, 131 Moo 5, Tiwnnont Road, Bangkadi, A. Maung, Pathum Thani, 12000, Thailand
Tel: 0-2501-3505-20 ext. 2021; Fax: 0-2501-3524; E-mail: viranee@siit.tu.ac.th, bunyarit@siit.tu.ac.th*

* Corresponding author

Suranaree J. Sci. Technol. 14(3):223-234

Many techniques have been purposed including detection of the OD regions by clustering the brightest pixels in retinal image and locating a potential OD area (Li and Chutatape, 2001). Other techniques have been recently proposed, based on a model of vascular structure (Foracchia *et al.*, 2004). They use a geometrical parametric model locating at the center point of the OD. Akita and Kuga (1982) trace the parent-child relationship between blood vessel segments, tracking back to the center of the optic disk. They also proposed robust detection of the blood vessels, which is difficult in images of a diseased retina where even quite sophisticated algorithms detect false positives along the edges of white lesions and along the optic disk. Lalonde *et al.* (2001) used pyramidal decomposition and a Hausdorff-based template matching that is guided by scale tracking of large objects using multi-resolution image decomposition. This method is effective, but rather complex. In three dimensional reconstructions of conventional stereo optic disk image procedures (Kong *et al.*, 2004), the resulting 3-dimensional contour images show optic disk structure clearly and intuitively, helping physicians in understanding the stereo disc photograph. Cox and Wood (1991) presented a semi-automated method to indicate external points on the boundary which were automatically connected by tracing along the boundary. Morris *et al.* (1993) initially presented a completely automatic method which traced between points on the boundary identified automatically by their grey level gradient properties. Sinthanayothin *et al.* (1999) used the rapid intensity variation between the dark vessels and the bright nerve fibers to locate the optic disk. However, we found that this algorithm often failed for fundus images with a large number of white lesions. Lee (1991) also applied an active contour model to high resolution images centered on the optic nerve head and his problem caused by the boundary of the pallor and by very faint or missing edges. Most of the techniques reviewed in this section were used to identify adults' well-formed optic disk. Only a few papers described techniques used to detect

OD in usually low-contrast infant images. We have tried a few techniques but they did not effectively detect the OD from the fundus image of an infant with ROP where the vessel and OD are not very well developed. Then we applied the technique of active contour to detect the boundary of the OD in low-contrast infant images.

Active contours, or Snakes, are curves defined within an image domain that can move under the influence of internal forces derived from the image data (Xu and Prince, 1997). The internal and external forces are defined so that the Snake will conform to an object boundary or other desired features within an image. Snakes are widely used in many applications, including edge detection (Grimson *et al.*, 1997), shape modeling (Terzopoulos, 1987), segmentation (Zijdenbos and Dawant, 1994) and motion tracking (Xu and Prince, 1998). Active contours, or Snakes, are used extensively in computer vision and image processing application, particularly to locate object boundaries. There are two key difficulties in the design and implementation of active contour models. First, the initial contour must, in general, be close to the wrong result. Second, active contours have difficulty progressing into boundary concavities. Xu and Prince (1997) developed a new external force, called gradient vector flow (GVF), which largely solves both problems. GVF is computed as a diffusion of the gradient vectors of a grey-level or binary edge map derived from the image. The resultant field has a large capture range, which means that the active contour can be initialized far away from the desired boundary. The GVF field also tends to force active contours into boundary concavities, where traditional Snakes have poor convergence.

Materials and Methods

Locating a First Snake with Optic Disk Location Approximation by Principal Component Analysis (PCA)

In order to place the first Snake on an image, the approximate location needs to be

found. A Principal Component Analysis (PCA)-based model was chosen to serve this purpose because it is very powerful in the detection of a similar shape to the trained shapes. The PCA-based model has been widely investigated in the application of face recognition (Gong *et al.*, 2000). The problem of optic disk location is similar to face detection in certain respects. The approach includes calculating the eigenvectors from the training images, projecting the new retinal image to the space specified by the eigenvectors and calculating the distance between the retinal image and its projection.

The first step of the PCA-based model is a training procedure to obtain 'disk space'. Fifty optic disk images are carefully selected as the training set. A square sub-image around the optic disk is manually cropped from each fundus image as training data. The sub-images are resized to $L \times L$ pixels and their intensities are normalized to the same range to form a training set. Each training image can be viewed as a vector of L^2 . L is the set to 90 in our application because most of the optic disk diameters from our test set are able to fit well into this square. The technique of PCA is applied to the training set to get the modes of variation around the average image. The

subspace defined by eigenvectors is termed as disk space. The model obtained by PCA statistical analysis is put to use in the localization of the optic disk in fundus images and explained in full detail as follows:

Step 1: Acquisition of Training Data Set

1.1) Optic disks were manually cropped, scaled to $L \times L$, and normalized. They were converted into a vector Γ_i of length $L \times L$. Fifty images were then transformed to a training set of $\{\Gamma_1, \Gamma_2, \Gamma_3, \dots, \Gamma_M\}$ where Γ_i is the vector of L^2 and M is 50 for our case (Figure 1).

Step 2: Definition of Disk Space

2.1) The average vector Ψ was computed using Eqn. (1), as demonstrated in Figure 2, and the set of deviation from the average vector $\Phi = [\Phi_1, \Phi_2, \dots, \Phi_M]$ is also defined with Eqn. (2):

$$\Psi = \frac{1}{M} \sum_{i=1}^M \Gamma_i \quad (1)$$

$$\Phi_i = \Gamma_i - \Psi \quad (2)$$

where Ψ = Average vector of the training set
 Φ = Difference between each training vector and the average vector

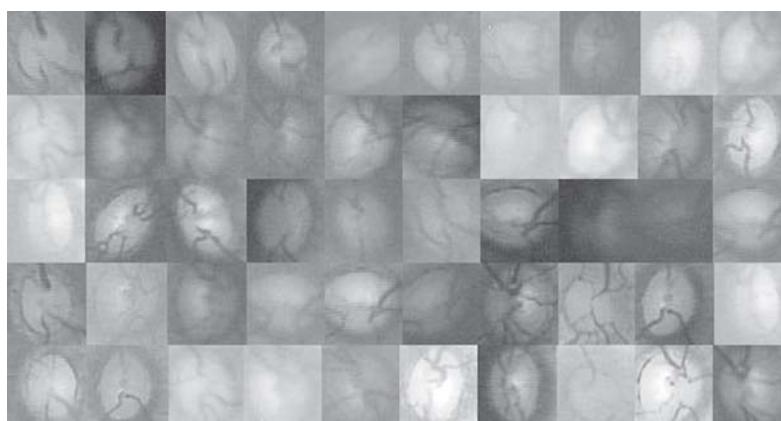


Figure 1. The training images of optic disk

2.2) A covariance matrix C which is defined in Eqn. (3) was computed in this step

$$C = \frac{1}{M} \sum_{i=1}^M \Phi_i \Phi_i^T \quad (3)$$

2.3) In this step, the vector u_k , as shown in Figure 3, is an eigenvectors (eigen disk) corresponding eigen value λ_k was calculated using Eqn. (4):

$$Cu_k = \lambda_k u_k \quad (4)$$

where u = The eigen vector (eigen disk) of covariance matrix C
 λ = The eigen value

2.4) A test image of original size of 640×480 pixels was raster scanned with a united block of $L \times L$ to form a Γ_{new} . It is later transformed into the disk space ω_k by the Eqn. (5.2):

$$\Phi_{new} = \Gamma_{new} - \Psi \quad (5.1)$$

$$\omega_k = u_k^T \Phi_{new} \quad (5.2)$$

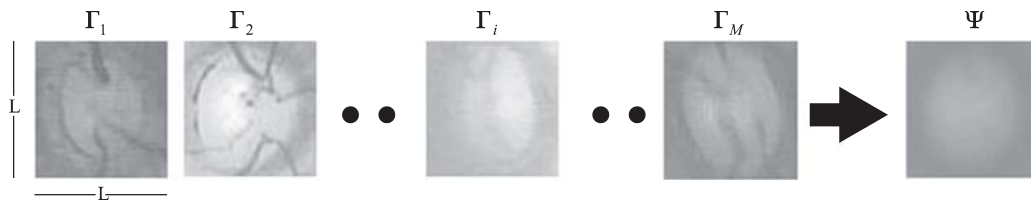


Figure 2. The training set of OD image and their average vector

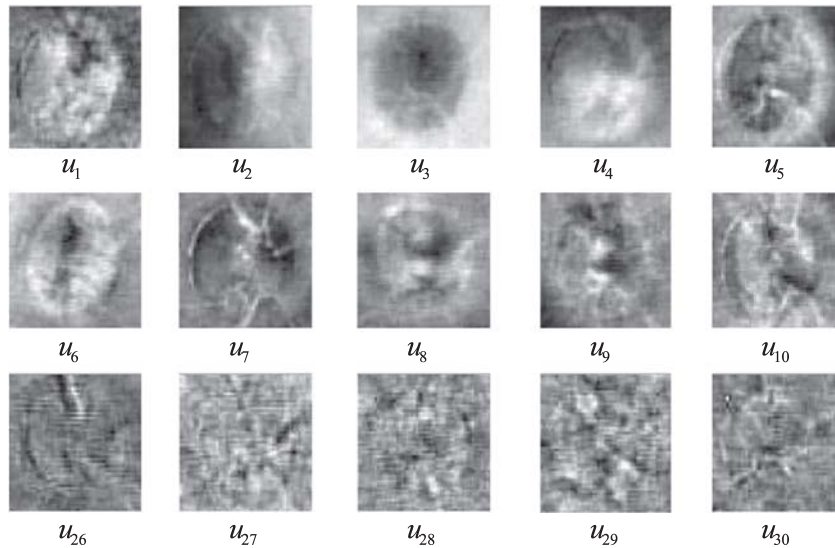


Figure 3. The examples of eigen disk

where $\omega_1, \omega_2, \dots, \omega_n$ are n new disk spaces (some of the examples are shown in Figure 4) and n is a number of selected dominant eigenvectors.

Step 3: Locating the Optic Disk

3.1) A pre-processed image is reconstructed by using its disk spaces and the eigen disks of the training set as shown in Eqn. (6):

$$\Phi_r = \sum_{k=1}^n \omega_k u_k \quad (6)$$

where Φ_r is a reconstructed image and n is the number of dominant eigen disk used in the previous step.

3.2) The sub-image will be classified as OD if the Euclidean distance between Φ_r and Φ_{new} , as expressed in Eqn. 7, is below a threshold value. The threshold value is derived from $\|\Phi_{new} - \Psi\|^2$. Some example results of optic disk detection are shown in Figure 5.

$$\mathcal{E}_{new} = \|\Phi_{new} - \Phi_r\| \quad (7)$$

All the processes in this step are summarized by a flowchart in Figure 6. The result from this step is quite successful; the algorithm can locate the OD with 80% accuracy compared with manual OD location from a test set of 50 images. The fail outcomes resulted from poor image quality or very blurred and unclassifiable OD.

Get Actual Shape of OD by GVF Snakes

Active contour, known as Snake, is the segmentation technique to detect the boundary of interest in an image. The Snake is a curve defined by $v(s,t) = [x(s,t), y(s,t)]$ in the x-y image plane, where s is a parameter corresponding on the curve, $s \in [0,1]$, and t as time.

In order to find the position of the Snake, the energy functional E_{snake} is represented as a sum of internal energy and external energy

$$E_{snake} = \int_0^1 [E_{int}(v(s,t)) + E_{ext}(v(s,t))] ds \quad (8)$$

where $E_{int}(v)$ represents the internal energy of the contour, and $E_{ext}(v)$ represents the external energy.

Because we need to extend the capture range of the Snake so that the Snake can find objects that are quite far away from the Snake's initial position, gradient vector flow or GVF (Xu and Prince, 1998) forces were then chosen because they derived from a diffusion operation and they tend to extend very far away from the object. The gradient vector flow (GVF) Snake, begins with the calculation of a field of forces, called the GVF forces, over the image domain. The GVF forces are calculated by applying generalized diffusion equations to both components of the gradient of an image edge map. The distance potential force is based on the principle that the model point should be attracted to the

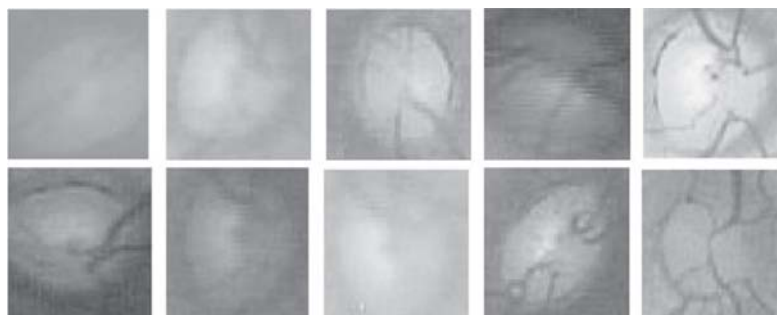


Figure 4. Examples of image reconstruction using eigen disk

nearest edge points. This principle, however, can cause difficulties when deforming a contour or surface into boundary concavities. Xu and Prince (1998) employed a vector diffusion equation that diffuses the gradient of an edge map in regions distant from the boundary, yielding a different force field called the gradient vector flow (GVF) field.

The amount of diffusion adapts according to the strength of edges to avoid distorting object boundaries.

The gradient vector flow (GVF) field $F_{ext}^{GVF} = h(x, y)$ is defined as

$$F_{ext}^{GVF} = h(x, y) = \begin{pmatrix} p(x, y) \\ q(x, y) \end{pmatrix} \quad (9)$$

The GVF field $h(x, y)$ is defined to minimize the following energy functional:

$$E_{GVF} = \iint_{x, y} \lambda \left[\left| \frac{\partial p}{\partial x} \right|^2 + \left| \frac{\partial p}{\partial y} \right|^2 + \left| \frac{\partial q}{\partial x} \right|^2 + \left| \frac{\partial q}{\partial y} \right|^2 \right] + |\nabla g|^2 |h - \nabla g|^2 dx dy \quad (10)$$

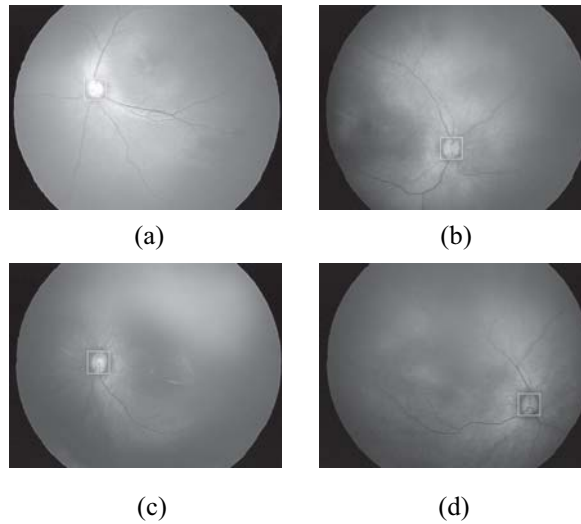


Figure 5. The detection results of 4 sample OD images

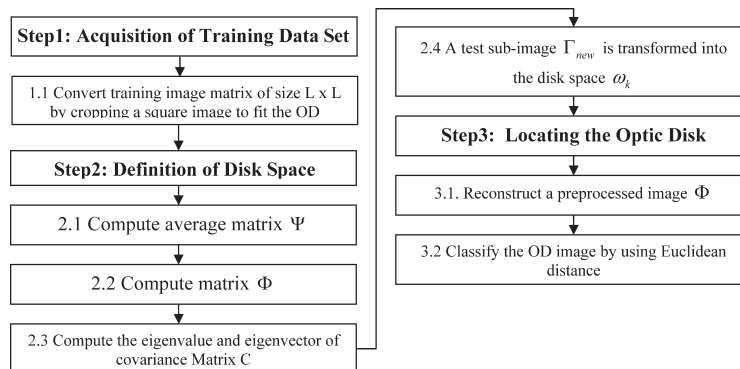


Figure 6. Showing a flowchart of PCA

where g is an edge map of the image and λ is the parameter governing the tradeoff between the first and second terms in integrand. Based on experiment result, λ is 0.5 for our case. Conversely, with near edges, where $|\nabla g|$ is large, the second term is dominant and can be regulated by setting $h \approx \nabla$ so that the local accuracy is preserved.

The implementation steps of using a GVF Snake to detect the OD boundary is as follows.

Step 1: The first Snake is placed near the image contour of interest as a result from the previous step. Figure 7(a) demonstrated the result.

Step 2: Find the Gradient Image. A simple Gaussian filter was applied on the image in order to get rid of the unwanted noise. This technique removes most of the noise and leaves the edge of OD boundary. Sigma of 2.5 was experimentally chosen. The result from this step is displayed in Figure 7(b).

Step 3: Generate GVF Force Field. The edge map was transformed into a gradient vector force field in this step. An external force field or gradient vector flow (GVF) field dense vector field derived from a gradient image by minimizing energy functional in a variation framework (Xu and Prince, 1998). The result from this step is shown in Figure 7(c).

Step 4: Snake Deformation. The shape of the Snake begins to deform in every iteration driving by forces applied on them. The iteration is repeated until the Snake is stable, the difference between two consecutive Snakes is lower than a threshold. An example of three steps is shown in Figure 7(d, e, f).

Step 5: Map the Resulting Snake to the Original Image. The boundary contour of the detected OD was mapped to the original image, as shown in Figure 7(g, h). This will facilitate the clinician's decision.

The whole process is summarized in Figure 8 and six more successful results are shown in Figure 9.

Results and Discussions

Fifty images with varying shapes and sizes of optic disk were used in this process.

These fifty images represent most of the cases of the ROP symptoms and they were sufficiently used to prove the concept of this algorithm. If the system is to be used in real situation, a bigger number of the images would be required. Apart from segmentation results from the GVF Snake, for comparison purposes, we also processed this set of images using a simpler 2D Circular Hough Transform. (This technique is based on a circular Hough Transform and the dimensions of the normal circular Hough Transform histogram are reduced from 3 to 2 dimensions by assuming that the approximate OD radius is known. Only the first few circles are evaluated by using the maximum point from Hough space). The detail of percentage of accuracy is shown in Figure 10.

Result Verification

The results were clinically validated in this step. All images in our test set were sent to an ophthalmologist to identify the OD manually. The expert ophthalmologist hand-labeled the optic disk on the screen. All optic disk pixels were set to white, and all non-optic disk pixels were set to black. The new image was saved as a ground truth which will be used for comparison. All the OD's which are automatically detected by our system are then compared with the clinician's hand-drawn ground truth. Figure 11 shows an example of both the ground truth image and our detection result. The hand-drawn and detected optic disk images are represented in white. The number of detected pixels that intersect with pixels of the hand-drawn ground truth will be summed and calculated as a percentage of pixels on the hand-drawn ground truth, as demonstrated in Table 1.

Accuracy Measurement

To evaluate the performance of the algorithm quantitatively, the measure of accuracy is defined as follow:

$$\text{Accuracy} = \frac{(TP+TN)}{(TP+FN+TN+FP)} \times 100 \quad (11)$$

where TP, TN, FP and FN stand for true positive, true negative, false positive and false

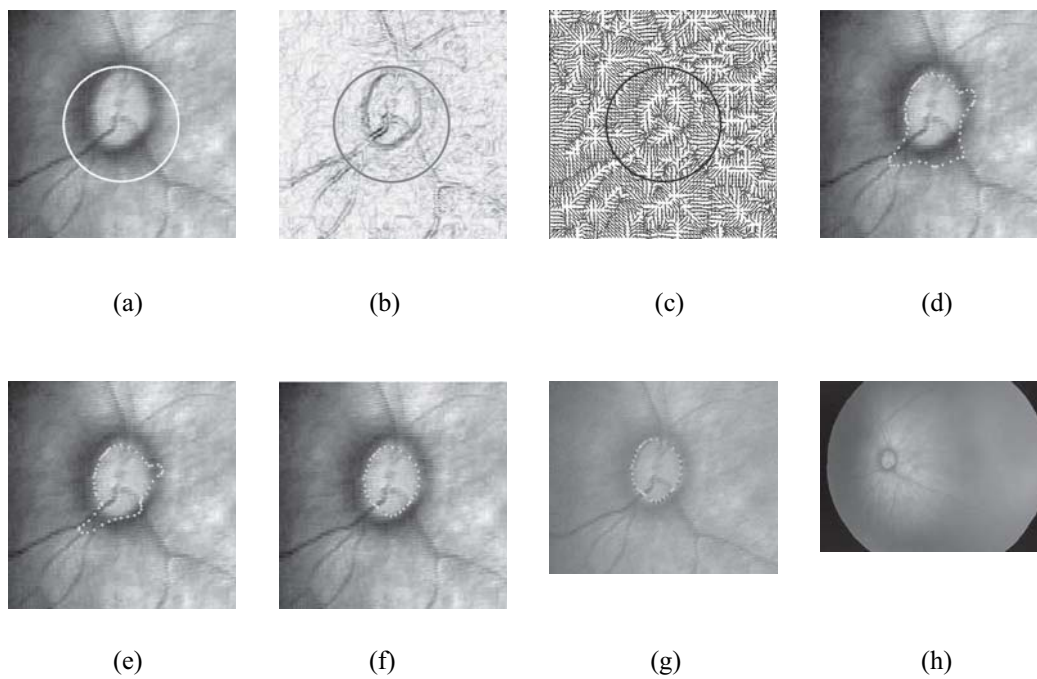


Figure 7. (a) The first Snake is placed near OD (b) The edge map $|G(x, y) * I(x, y)|^2$ with $\sigma = 2.5$ (c) GVF field image (d), (e), (f) An example of GVF Snake in action where (d) Initial position of Snake and location of the model after 40 (e) 80 and (f) 200 iterations (g), (h) Detected OD is mapped to the original fundus image

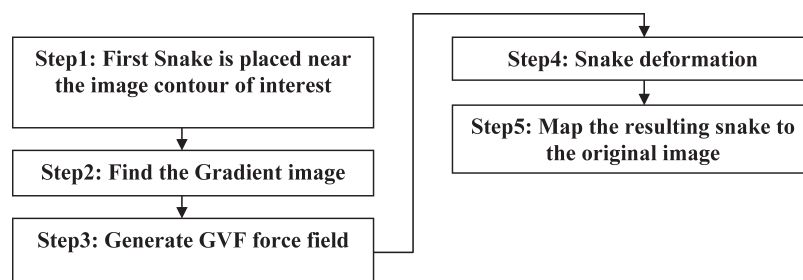


Figure 8. A flowchart of GVF Snake

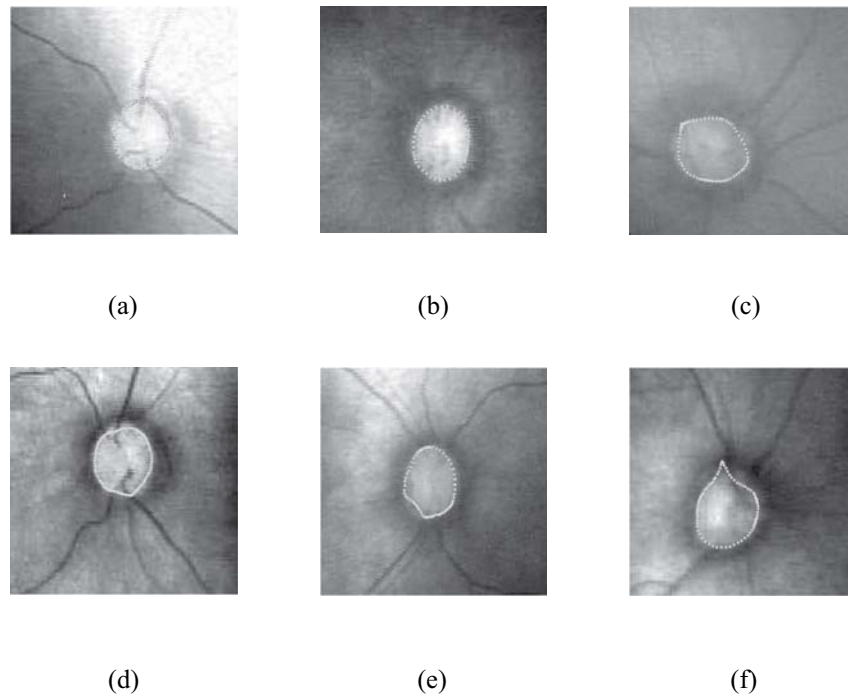


Figure 9. Examples of successful results

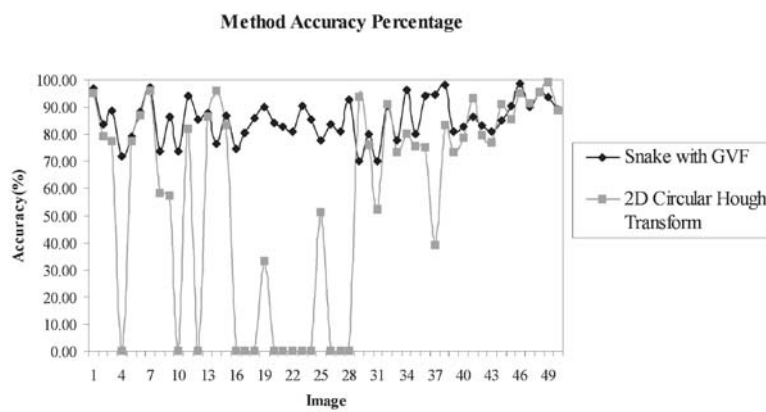


Figure 10. The accuracy result for all images

negative, respectively (Costaridou, 2005). An example of the comparison is demonstrated in Figure 12.

Conclusion

We have presented a method for optic disk detection based on a PCA and GVF Snake. The method was implemented on Pentium 4, 3 GHz machine with 1 GB of RAM and the speed of transform is approximately 10 sec/image. Because the algorithm will stop when there are no changes in the accuracy, i.e. when the result is converged. From our experiment, approximately it will converge after 10 sec for each

image. The Rate of Convergence for each image is 10 sec. The PCA was used to get a rough location of the OD, and the first GVF Snake was placed closely to the center of the optic disk. The GVF Snake then followed the external vector force field until it fitted the boundary of the OD. The results were compared with the result from a 2D Circular Hough Transform and validated against a clinician's hand-drawn ground truth. The accuracy result is quite successful with accuracy of 85.3% compared to the accuracy result of Circular Hough Transform which is 56.9%. One visible advantage of this method is that the ODs are detected even though the boundary of the OD is not continuous or blurred.

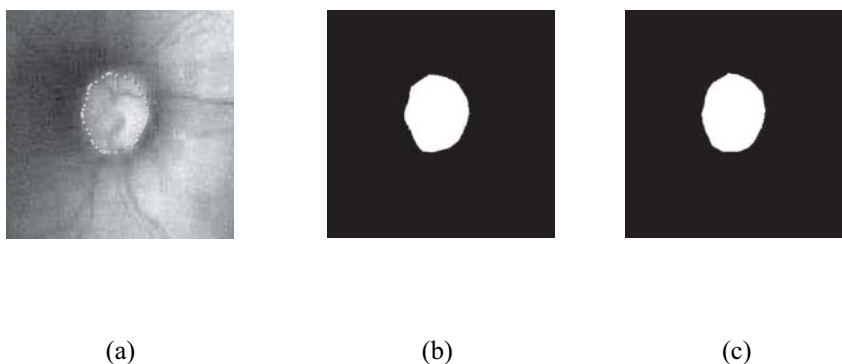


Figure 11. (a) OD automatically detected by our system (b) Detected pixels (c) Clinician's hand-drawn ground truth

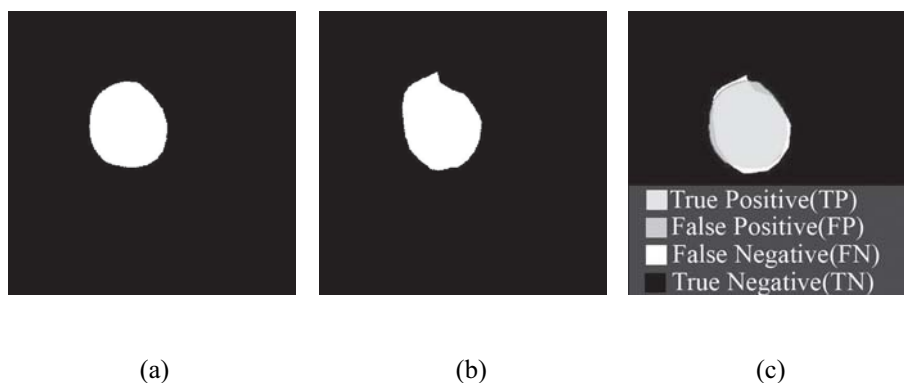


Figure 12. (a) Ground truth image (b) Detected pixels (c) Definition of segmentation evaluation

Table 1. Some examples of comparison results of intersected pixels on some selected images

Image ID	Image Name	Ground truth pixels	Detected pixels from Snake with GVF	Detected pixels from Hough Transform	Snake Accuracy (%)	2D Circular Hough Transform Accuracy (%)
1	A1	7,891	7,625	7,487	96.6	94.9
2	A2	7,466	6,257	5,896	83.8	79.0
3	A3	6,174	5,474	4,783	88.7	77.5
4	A5	8,628	6,181	0	71.6	0.0
5	A6	7,453	5,890	5,763	79.0	77.3
6	A7	8,658	7,624	7,526	88.1	86.9
7	A9	5,470	5,321	5,240	97.3	95.8
8	B2	14,481	10,670	8,401	73.7	58.0
9	B3	12,649	10,943	7,216	86.5	57.1
10	B6	7,099	5,230	0	73.7	0.0
11	B8	9,254	8,728	7,576	94.3	81.9
12	B10	9,203	7,878	0	85.6	0.0
13	C2	8,393	7,373	7,236	87.9	86.2
14	C5	7,776	5,927	7,462	76.2	96.0
15	C6	8,587	7,441	7,135	86.7	83.1
16	C7	8,438	6,278	0	74.4	0.0
17	C8	7,879	6,330	0	80.3	0.0
18	C9	7,520	6,469	0	86.0	0.0
19	C10	7,615	6,842	2,544	89.9	33.4
20	C11	7,551	6,356	0	84.2	0.0
21	C12	7,509	6,228	0	82.9	0.0
22	C13	8,155	6,612	0	81.1	0.0
23	C14	6,494	5,863	0	90.3	0.0
24	D1	7,029	6,010	0	85.5	0.0
25	D3	14,175	11,002	7,291	77.6	51.4
26	D4	8,513	7,113	0	83.6	0.0
27	D11	8,937	7,213	0	80.7	0.0
28	D14	10,644	9,854	0	92.6	0.0
29	E2	7,517	5,270	7,037	70.1	93.6
30	E3	9,581	7,674	7,268	80.1	75.9
31	E6	14,075	9,854	7,356	70.0	52.3
32	E7	8,077	7,298	7,360	90.4	91.1
33	E9	9,935	7,710	7,267	77.6	73.2
34	G1	9,096	8,761	7,268	96.3	79.9
35	G2	9,682	7,747	7,296	80.0	75.4
36	G3	9,611	9,036	7,221	94.0	75.1
37	G4	9,484	8,978	3,703	94.7	39.0
38	G5	8,648	8,497	7,180	98.3	83.0
39	G6	9,768	7,885	7,147	80.7	73.2
40	G8	7,004	5,782	5,521	82.6	78.8
41	G9	7,929	6,864	7,375	86.6	93.0
42	G10	6,670	5,562	5,320	83.4	79.8
43	G11	7,147	5,769	5,478	80.7	76.7
44	G12	7,872	6,704	7,172	85.2	91.1
45	G14	6,220	5,622	5,312	90.4	85.4
46	G15	7,685	7,577	7,303	98.6	95.0
47	G16	7,882	7,108	7,193	90.2	91.3
48	G17	7,435	7,097	7,113	95.5	95.7
49	G18	7,622	7,154	7,558	93.9	99.2
50	G19	8,057	7,182	7,138	89.1	88.6
Average Percentage					85.3	56.9

Acknowledgements

We would like to express our thanks to Dr. Sarah Barman at Kingston University, UK, for her support and images provided for this project.

References

- Akita, K. and Kuga, H. (1982). A computer method of understanding ocular fundus images. *Pattern Recognition*, 5(6):431-443.
- Costaridou, L. (2005). *Medical Image Analysis Methods*. CRC Press, NY, p. 438-440.
- Cox, M.J. and Wood, I.C.J. (1991). Computer-assisted optic nerve head assessment. *Ophthal. Physiol. Opt.*, 11:27-35.
- Foracchia, M., Grisan, E., and Ruggeri, A. (2004). Detection of optic disc in retinal images by means of a geometrical model of vessel structure. *IEEE Transactions on Medical Imaging*, 23(10):1,189-1,195.
- Gong, S., McKenna S.J., and Psarrou, A. (2000). Dynamic vision from images to face recognition. Imperial College Press, London, p. 297-300.
- Grimson, W.E.L., Ettinger, G.J., Kapur, T., Leventon, M.E., Wells, W.M., and Kikinis, R. (1997). Utilizing segmented MRI data in image-guided surgery. *Int'l J. Patt. Recog. Artificial Intell.*, 11(8):1,367-1,397.
- Kong, H.J., Kim, S.K., Seo, J.M., Park, K.H., Chung, H., Park, K.S., and Kim, H.C. (2004). Three dimensional reconstruction of conventional stereo optic disc image. *Annual International Conference of the IEEE EMBS*; September 1-5, 2004; p. 1,229-1,232.
- Lalonde, M., Beaulieu, M., and Gagnon, L. (2001). Fast and robust optic disk detection using pyramidal decomposition and Hausdorff-based template matching. *IEEE Transactions on Medical Imaging*, 20(11):1,193-1,200.
- Lee, S. (1991). Visual monitoring of glaucoma. Ph.D. Robotics Research Group, Department of Engineering Science, University of Oxford, Available on micro-fiche.
- Li, H. and Chutatape, O. (2001). Automatic location of optic disk in retinal images. *Proceedings of IEEE-ICIP*; October 7-10, 2001; Thessaloniki, Greece, p. 837-840.
- Moris, D.T., Cox, M.J., and Wood, I.C.J. (1993). Automated extraction of the optic nerve head rim. *American Association of Ophthalmologists Annual Conference*; December 1993; Boston, p. 11-12.
- Sinthanayothin, C., Boyce, J.F., Cook, H.L., and Williamson, T.H. (1999). Automated localization of the optic disc, fovea, and retinal blood vessels from digital color fundus images. *Br J. Ophthalmol.*, 83(8):902-910.
- Terzopoulos, D. (1987). On matching deformable models to images. Technical Report 60, Schlumberger Palo Alto research, 1986. Reprinted in *Topical Meeting on Machine Vision, Technical Digest Series*, 12:160-167.
- Xu, C. and Prince, J. L. (1997). Gradient vector flow: a new external force for snakes. *Proceedings of IEEE Conf. on Comp. Vis. Patt. Recog. (CVPR)*; June 1997; Los Alamitos, p. 71.
- Xu, C. and Prince, J.L. (1998). Snakes, shapes, and gradient vector flow. *IEEE Trans Imag. Proc.*, 7(3):359-369.
- Zijdenbos, A.P. and Dawant, B.M. (1994). Brain segmentation and white matter lesion detection in MR images. *Critical Reviews in Biomedical Engineering*, 22(5-6):401-465.